

Analysis of Fasteners as Disbond Arrest Mechanism for Laminated Composite Structures

Chi Ho E. Cheung^{*}, Phillip M. Gray[†], Gerald E. Mabson[‡] and Kuen Y. Lin[§]

University of Washington, Seattle, WA, 98195-2400

An FEA model for understanding the effectiveness of fastener as crack arrest mechanism has been constructed. The effect of the fastener in the sliding direction (Mode II) is modeled using fastener flexibility approach. The FEA results show that the fastener provides significant crack retardation capability in both Mode I and Mode II conditions. The analyses provide insights into the problem of disbond/delamination arrest using fastener or similar mechanisms.

An analytical model for the problem is developed. The model consists of a split-beam with a fastener attached; the fastener is modeled as a system of springs. An elastic layer is placed between the beams on the cracked faces to resolve contacts. The problem is solved using energy principles. The mode-decomposed strain energy release rates (SERR) at the crack tip are solved analytically¹¹⁻¹³.

The primary goal of the current work is to enhance the safety of bonded composite structures by providing analysis methods for arrest mechanism.

^{*} Research Assistant, Department of Aeronautics and Astronautics, University of Washington, Seattle, WA

[†] Research Assistant, Department of Aeronautics and Astronautics, University of Washington, Seattle, WA

[‡] Technical Fellow, The Boeing Company, Seattle, WA

[§] Professor, Department of Aeronautics and Astronautics, University of Washington, Seattle, WA

I. Introduction

The use of composites in aircraft has enabled the use of bonded (co-cured, co-bonded or secondary bonding) structures, the main advantages of which are reduction of part counts and weight. The critical damage mode in this type of structure is disbond (and substrate delamination) due to impact damage. Complete disbonding of components (e.g. skin-stringer shown in Figure 1) can cause failure at the structural level even though the individual components remain intact. Therefore, any bonded structures must demonstrate fail-safety by providing adequate crack (including disbond and delamination) arrest capability to ensure safety.

The bond line alone, which is the primary load path, seldom possesses necessary arrest capability. This can be a difficult problem when designing the structure to be fail-safe because any crack propagation will result in catastrophic separation of the parts. In aircraft structures, it is common to use fasteners for assembly of geometrically complex configurations (e.g. fuselage skin-frame shear tie). These fasteners are co-located with the skin-stringer bond, and thus also perform as disbond arrest mechanism without the added cost and complexity of alternatives such as z-pin and z-stitching. Alternatively, fasteners or similar features may be added along a bond line for the sole purpose of crack arrestment; these fasteners would carry no load unless damage reaches their location. A possible extended application is to install fasteners at a damaged location on a structure in service to prevent further propagation, instead of extensive repairs that is both expensive, time consuming and decreases dispatch reliability of a servicing structure.

Disbond in Mode I is well understood and typically less problematic because it is easy to design an arrest feature that would be sufficiently effective; other failure modes are likely to occur before the failure of the arrest feature, e.g. laminate bending, fastener pull through. However, Mode II crack arrest mechanism is less well understood. It is therefore important to understand the effectiveness of these fasteners in arresting disbond to maximize their benefits and ensure safety of the structure. This paper will focus on the investigation of the behavior of fastener as crack arrest mechanism and the development of analytical methods to analyze the problem.

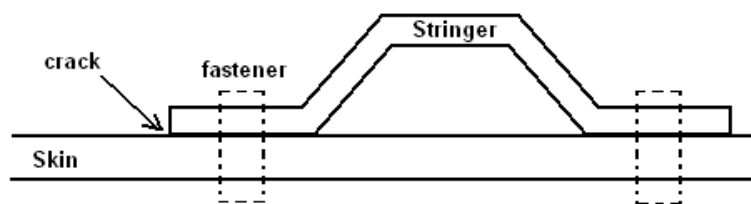


Figure 1. Schematic of Damaged Fuselage Skin-Stringer with Fastener

II. Fastener Effectiveness as Disbond Arrest Mechanism – FEM

The load case, shown in Figure 2, represents the typical condition in which the fastener would perform as a crack arrest mechanism. For example, the lower plate represents the fuselage skin while the upper plate represents a stringer leg. A crack (disbond, delamination, etc) exists at the edge of the skin-stringer bond. The overhanging portion of the stringer leg is free from any load, while the skin is loaded with general axial tension (N) and moment (M) loads. This configuration is generalized as an analytical model shown below in Figure 3. The model consists of a split-beam, with the crack tip at the connecting end of the beams. A system of springs attaches to the

beams at a given location to represent the elastic behavior of the fastener or the crack arrest feature. General far field loads are applied to the beams at the free ends. As the crack advances to the fastener location, the fastener would arrest or retard the growth of the crack. A proper design should be capable of arresting or retarding the crack up to limit load or until other failure modes occur, such as bending, bearing, fastener pull-through, etc. Therefore, failure would be defined as the excessive continual advancement of the crack below the critical loads of the other failure modes. The critical loads of the other failure modes and how they interact with the effectiveness of the fastener is beyond the scope of this paper.

The conventional notion of “crack length” requires minor adjustment in understand in the current study; while the crack length is traditionally defined as the length of the separated part of the beams or model, the crack length of interest is only the length between the crack tip and the fastener.

Initially, 2-D finite element analyses (FEA) using Abaqus are performed to acquire necessary understanding of the mechanisms pertaining to the fastener as a crack arrest mechanism. Contact between the beams is modeled by contact elements, i.e. infinite stiffness when interference is detected and zero stiffness otherwise. The crack propagation is analyzed using Virtual Crack Closure Technique (VCCT), which evaluates mode-decomposed strain energy release rate of the crack. Fastener flexibility approach by Huth⁵ is used to model the axial elastic behavior of the fastener-beams joint. Contact friction is not modeled currently as the magnitude is small compared to the far field loads needed to propagate the crack. Fastener preload is also not modeled, though it will be in the future. The effect of ignoring fastener preload will be discussed.

Thermal stress is not considered in this study as the upper and lower beams are made identical. The understanding obtained from the FEA results became the foundations of the analytical model under development, which aims to provide the computational efficiency orders of magnitude higher than FEA.

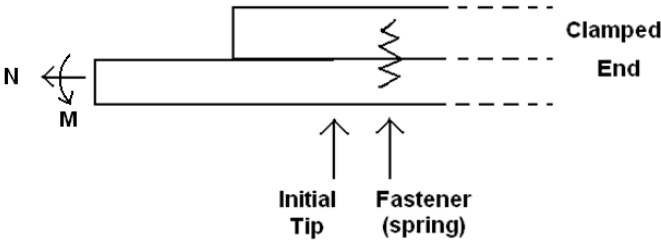


Figure 2. Typical Load Case of Fastener as Disbond Arrest Mechanism

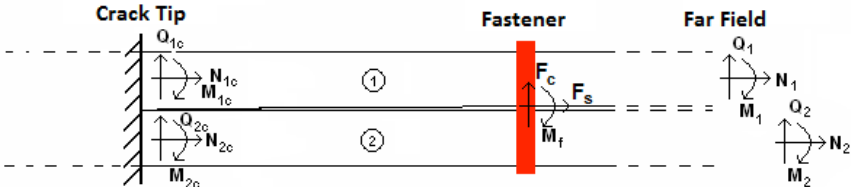


Figure 3. Double Cantilever Beam with Fastener Analytical Model

A. Structural Properties

The model used in the FEA portion of the study reflects the configuration shown in Figure 2. As shown in the figure, loads are only applied to one of the beams. A 16-ply laminate with identical lay-up is used for both beams. Four composite laminate lay-ups are used in the current study (Table 3), ranging from quasi-isotropic (25% 0-deg) to 62.5% 0-deg for high stiffness. Quasi-isotropic lay-ups are suitable for fuselage skins under multi-axial loads; high stiffness lay-ups are suited for stringers/stiffeners.

AS4/3501-6 material properties used are summarized in Table 1 ^{6,7}. B-K law (1), with mixed-mode fracture parameter η , is used to determine crack propagation behavior ⁷. Material properties for Ti-Al6-V4 titanium fastener for aircraft applications are summarized in Table 2.

$$G_{equivC} = G_{IC} + (G_{IIC} - G_{IC}) \left(\frac{G_{II}}{G_I + G_{II}} \right)^\eta \quad (1)$$

Table 1 – Composite Lamina Material Properties (AS4/3501-6)

	English Units	SI Units
thickness	0.0075in	0.1905mm
E_1	18.5×10^6 psi	127.5GPa
$E_2 = E_3$	1.64×10^6 psi	11.3GPa
$G_{12} = G_{13}$	0.871×10^6 psi	6.0GPa
G_{23}	0.522×10^6 psi	3.6GPa
$\nu_{12} = \nu_{13}$	0.3	0.3
ν_{23}	0.4	0.4
G_{IC}	1.5 lb/in	0.2627N/mm
G_{IIC}	7 lb/in	1.226N/mm
η	1.75	1.75

Table 2 – Titanium Fastener Properties (Ti-Al6-V4)

diameter	0.25in	6.35mm
E	16.5×10^6 psi	114GPa

The effect of fastener is modeled using fastener flexibility approach (Huth⁵). The equation for compliance of the fastener in un-bonded bolted joints in the sliding direction (Mode II) was obtained from empirical data given by equation (2). The parameters used are: t_i = laminate thickness, d = fastener diameter, n = number of fasteners ($n = 1$), $E_{1,2}$ = laminate stiffness, E_3 = fastener stiffness, constants $a = 2/3$ and $b = 4.2$ for bolted graphite/epoxy joints. The fastener flexibilities, k_{II} , for the different composite laminate lay-ups considered are summarized in Table 3. The four lay-ups, ranging from quasi-isotropic to 62.5% 0-deg, are determined using common rules for stacking sequence in aircraft applications. For example, use 45° on the outside to protect the load bearing 0° plies, put 0° plies on the outside for maximum bending stiffness, group no more than 3 plies of the same orientation together to minimize interlaminar stresses, etc. In the opening direction (Mode I), a stiffness of $k_I = E_3 \times \text{Area} / (t_1 + t_2) = 591.0 \times 10^3$ N/mm (3.37×10^6 lb/in) is used.

$$C = \left(\frac{t_1 + t_2}{2d} \right)^a \frac{b}{n} \left(\frac{1}{t_1 E_1} + \frac{1}{n t_2 E_2} + \frac{1}{2 t_1 E_3} + \frac{1}{2 n t_2 E_3} \right) \quad (2)$$

Table 3 – Fastener Flexibility for Different Composite Laminate Lay-ups

	k_{II} (lb/in)	k_{II} (N/mm)
25.5% 0-deg - (45/0/-45/90/45/0/-45/90) _s	141.17×10^3	24.72×10^3
37.5% 0-deg - (45/0/-45/0/45/0/-45/90) _s	168.93×10^3	29.58×10^3
50.0% 0-deg - (45/0 ₂ /-45/0 ₂ /90 ₂) _s	192.25×10^3	33.67×10^3
62.5% 0-deg - (45/0 ₃ /-45/0 ₂ /90) _s	217.32×10^3	38.06×10^3

B. FEA Model

The skin-stringer configuration is modeled in 2-D in commercial FEA software Abaqus (Figure 3). The model is identical to a double cantilever beam (DCB) except that only the lower beam is loaded while the upper beam is free. The disbond (crack) is at the interface between the skin and stringer within the matrix material. The beams are $L = 127\text{mm}$ (5in) long. Initial crack length is $a_0 = 50.8\text{mm}$ (2.0in) or $a/L = 0.4$. The springs representing the fastener are located at $l_{\text{fast}} = 63.5\text{mm}$ (2.5in). These springs are inactive until the crack tip reaches l_{fast} . Plane strain quadrilateral elements reduced integration with hourglass control is used. Each ply is modeled with one element through the thickness; element length is 0.254mm (0.01in) in the longitudinal direction. Same element size is used for the entire beam in order to maintain consistency as the crack propagates along the length of the beam. Load is applied at the lower beam at the mid-plane. Geometric nonlinearity is considered.

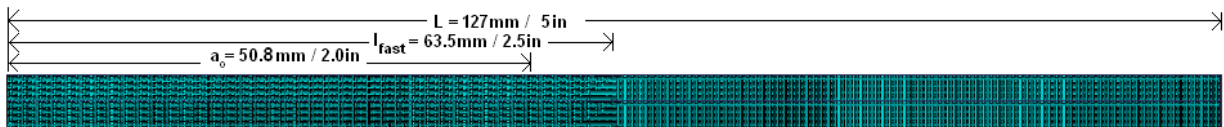


Figure 3. FE Mesh the Split Beam Model

Crack propagation is modeled using Virtual Crack Closure Technique elements in Abaqus⁸. Strain energy release rate for each mode is calculated separately using the nodal forces at the crack tip and displacement behind the crack tip for the corresponding mode. The crack propagates to the next node when the mixed-mode fracture criterion (1) is met.

The fastener is modeled with two separate springs acting in two independent directions. In the opening direction or Mode I, a spring acting only in y-direction with stiffness $k_I = E_3 \times \text{Area} / (t_1 + t_2)$ is used. In the sliding direction or Mode II, a spring acting only in x-direction with stiffness $k_{II} = 1/C$ (C is joint compliance from equation (2)) is used. The fastener flexibility calculations assume width of 25.4mm (1.00in), or fastener spacing of 4×fastener diameter. No failure points for the springs are defined.

In the current study, thermal residual stresses are not considered because the upper and lower beams have identical stacking sequence. In general, thermal residual stresses would be considered since stringers usually have higher stiffness than skins.

C. FEA Results and Discussions

The FEA results for crack propagation behavior with and without crack arrest mechanism is presented as follows. Only pure tension (figures 4 and 6) and pure moment load (figures 5 and 7) cases are shown (load cases refer to Figure 2). The crack length versus load magnitude results demonstrate the effectiveness of the arrest mechanism in retarding crack propagation; the strain energy release rate (SERR) components versus crack length results reveal the changes in fracture characteristics due to the presence of the arrest mechanism.

Figures 4 and 5 show the absolute crack length versus load magnitude plots for pure tension and pure moment load cases. The analyses start at crack length of 50.8mm, where the arrest feature has no effect on crack propagation. The location of the fastener is at 63.5mm, beyond which the effectiveness in crack retardation can be observed. A vertical line in these plots implies unstable crack propagation; a horizontal line implies

no crack propagation; and a line with positive slope implies stable crack propagation. In general, the crack length vs. load curves can be divided into three sections: 1) crack not yet reached the fastener; 2) crack being retarded by the fastener; and 3) crack continue to advance pass the fastener. It should be noted that the FEA model has a finite length of 127mm, the clamped boundary begins to affect the crack tip after crack length of 115mm, after which the results are discarded.

In figure 4, results for pure tension load on the lower beam, it can be seen that crack propagation is stable with and without arrest mechanism. This is counterintuitive because crack propagation should be unstable under applied load; however, crack propagation is stable because of nonlinear geometric deformation, i.e. rotation of the crack tip when tension is applied to the neutral axes of the lower beam, below plane of symmetry of the model. In fact, for a finite length model and this particular load case, crack propagation is stable for crack length of approximately $a > 0.35L$ and unstable for $a < 0.35L$ (behavior similar to that of an end-notched flexure specimen). The presence of a fastener demonstrates significant crack retardation effectiveness; the crack length vs. load curves show large horizontal sections, meaning almost no crack propagation for significant load increase. At the end of the horizontal sections, the cracks continue to propagate with behavior similar to that of cases without fastener. The end of the horizontal section may be used to define the limiting capability of the arrest mechanism, as the crack propagation afterwards is essentially unstable. In all lay-ups, the crack is held within 6.35mm of the fastener location before failure as defined above; this is a reasonable value this is the same as the fastener diameter. The fastener provides

approximately 50% load carrying capability enhancement over the cases without fasteners for all four lay-ups.

In figure 5, results for pure moment load on the lower beam, it is shown that the presence of a fastener has significant crack retardation capability; the large sections of horizontal curves are clearly present, meaning almost no crack propagation. In all lay-ups, the crack is held within 3.8mm of the fastener location before failure. The fastener is capable of arresting the crack for additional 17.5N-m, 19.2N-m, 21.5N-m and 22.0N-m of moment for the 25%, 37.5%, 50% and 62.5% 0-deg lay-ups respectively. This is equivalent to an average of 190% load carrying capability enhancement over the cases without fasteners. The sensitivity of results to difference in lay-up is much smaller in the case of applied moment compared to that of applied tension.

Figures 6 and 7 shows the SERR components versus load magnitude plots for pure tension and pure moment load cases. There two curves for each case, showing G_I and G_{II} at the crack tip at the moment of propagation. These SERR components correspond to the values required to satisfy the mixed-mode fracture law (1) for crack propagation. The SERR components vs. crack length curves can correspondingly be divided into three sections similar to the crack length vs. load curves. The FEA results are affected by the clamped boundary condition after crack length of 115mm, after which the results are discarded.

Figure 6 shows the results for pure tension. Without the influence of the fastener, the crack propagation is of mixed-mode type, even though the external load applied is pure Mode II. The nonlinear geometric deformation, resulting in the rotation of the crack tip, adds Mode I component to the crack tip. As the crack advances past the fastener, the

opening displacement is essentially eliminated by the relatively high axial stiffness of the fastener, thus eliminating G_I . In order for the crack to continue to advance, G_{II} has to increase to compensate. Since G_{IIC} is much higher than G_{IC} , a large increase in load magnitude is required create sufficient G_{II} to advance the crack. The horizontal sections representing retardation of the crack in figures 4 and 5 directly correspond to the section representing the transition from mixed-mode fracture to pure Mode II fracture as illustrated in figure 6 (and figure 7).

Figure 7 shows the results for pure moment, which have very similar behavior as that for pure tension. Without the influence of the fastener, the crack propagation is of mixed-mode type, even though the external load applied is pure Mode I. The fastener eliminates opening displacement of the crack tip, thus eliminating G_I . Subsequent crack propagation is only in Mode II.

It is evident that the primary mechanism for crack retardation by fastener is by eliminating opening displacement, thus eliminating G_I , and forcing the crack to propagate in pure Mode II. In doing so, the load required for crack propagation increases significantly, achieving the desired effect of crack arrestment. The benefit from fracture mode transition (mixed mode to pure Mode II) is much larger than that from the elastic resistance of the fastener itself. Load cases traditionally resulting in significant G_I at the crack tip receive the greatest benefits; load cases resulting in pure G_{II} may only benefit by the relatively low fastener joint stiffness. The presence of a fastener, regardless of load case, is drastically better than the catastrophic unstable crack growth expected in structures without a proper arrest mechanism.

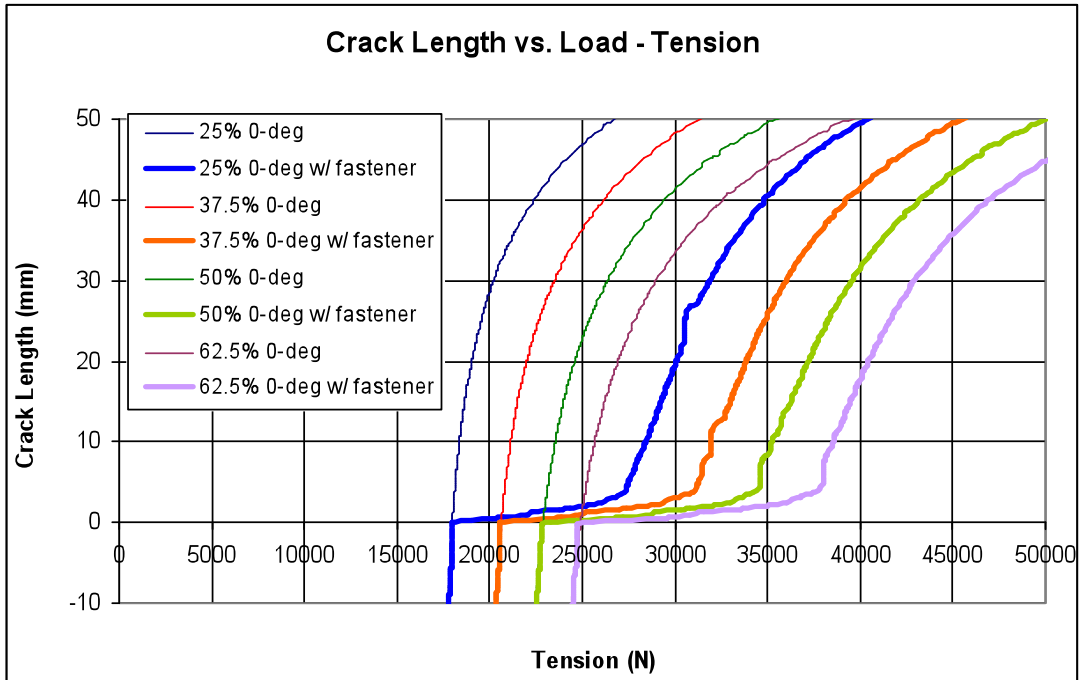


Figure 4. Crack Length versus Load w/ and w/o Fastener –Tension on Lower Beam

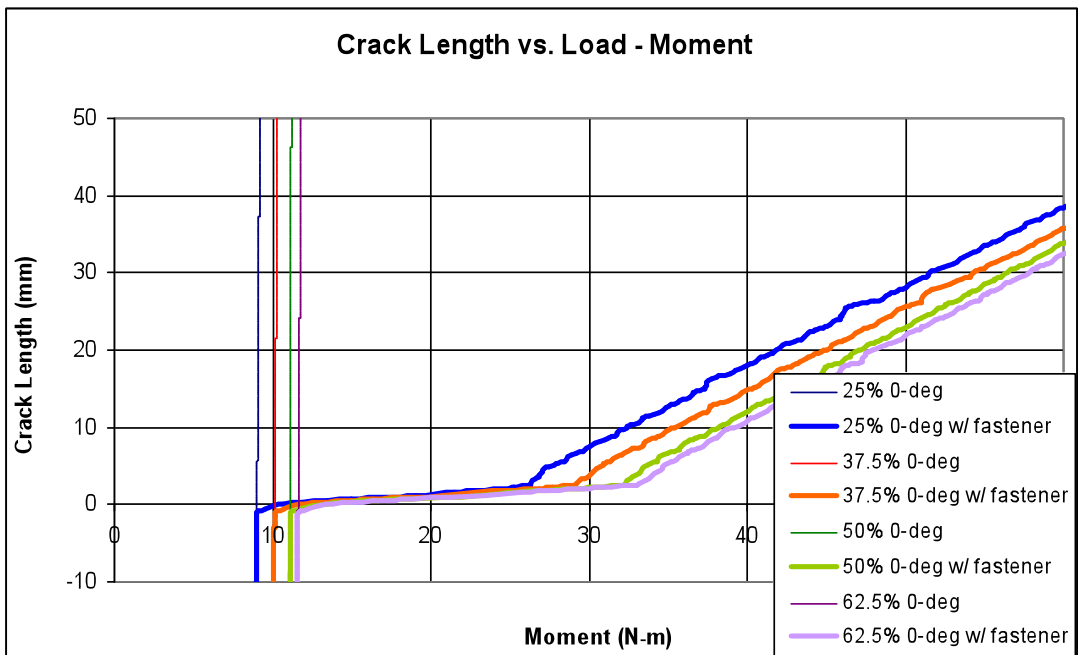


Figure 5. Crack Length versus Load w/ and w/o Fastener – Moment on Lower Beam

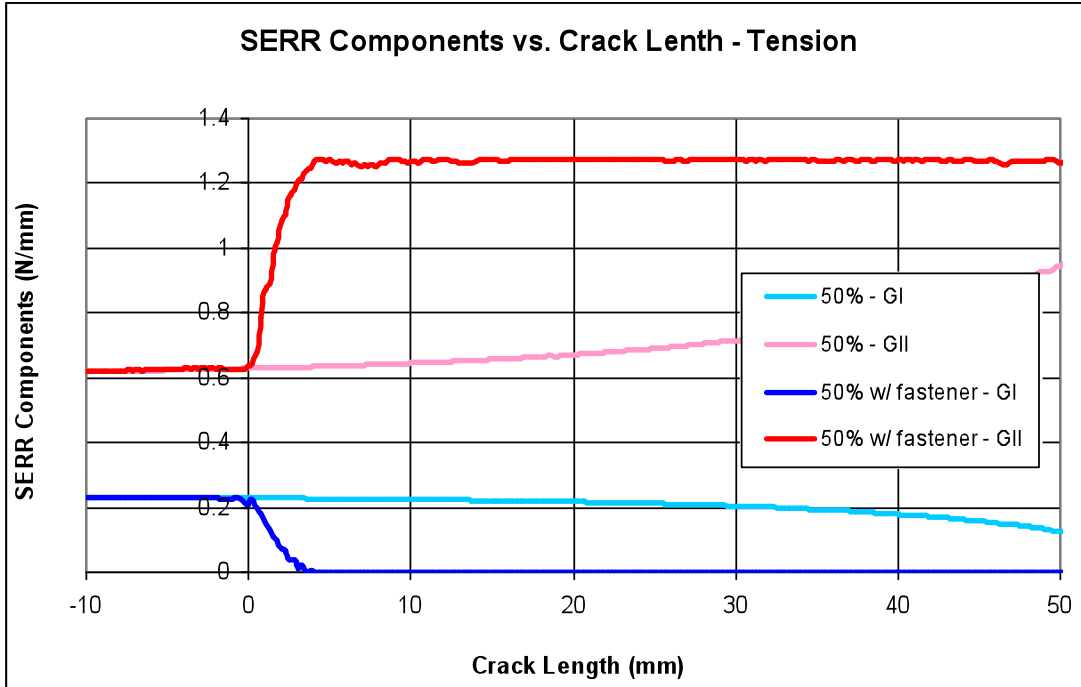


Figure 6. G_I and G_{II} vs. Crack Length w/ and w/o Fastener – Tension on Lower Beam

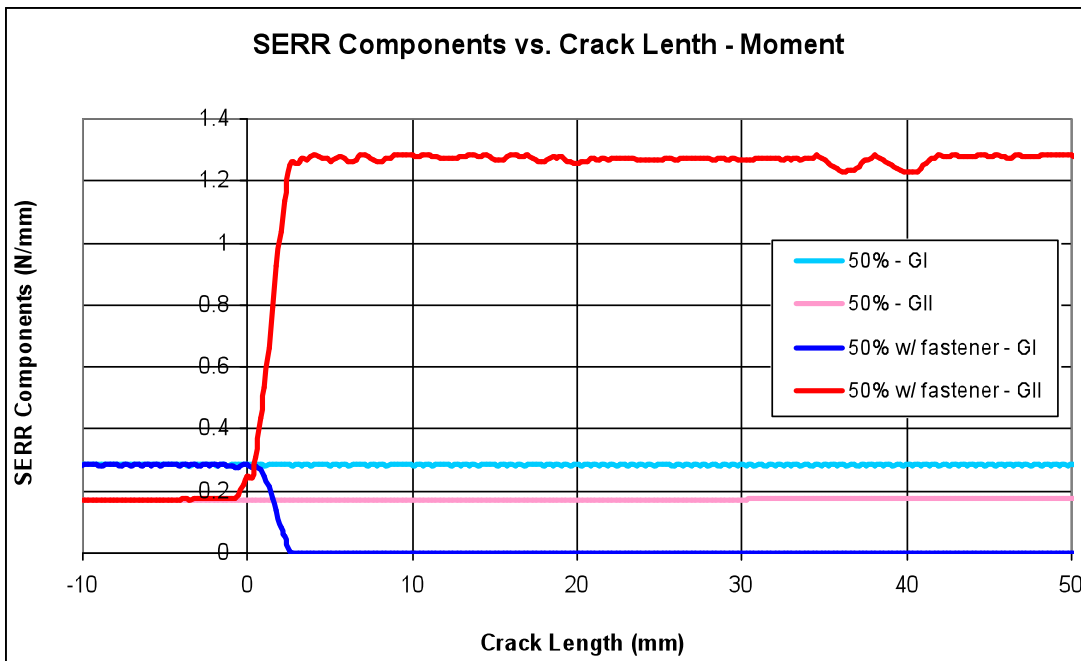


Figure 7. G_I and G_{II} vs. Crack Length w/ and w/o Fastener – Moment on Lower Beam

The effect of fastener preload and contact friction are also investigated in Abaqus. The FE model used is identical to the one described previously. A 62.5% 0-deg layup is used for both laminates, each with an ultimate load of 34.7kN (7800lb) at 5000 micro-strain. A fastener diameter 6.35mm (0.25in) with tensile yield load of 32.75kN (7363lb) is used. A value of 0.5 is assigned for the crack face friction coefficient. The load case is equal and opposite axial loads ($N1 = - N2$), which produces pure Mode II SERR at the crack tip. The results are shown in Figure 8 below; the applied load is normalized to the laminate strain failure load and the fastener preload is normalized to the fastener tensile yield load.

It can be seen that for the cases with various preload values (0 to 75%) without friction, no visible difference in crack propagation behavior can be observed. This is expected because the load case used is pure Mode II, adding more resistance to Mode I by providing fastener preload should not have any effect. For cases where friction is added, appreciable crack retardation benefits can be observed; the crack retardation benefits increases for increasing preload. However, it should be noted that the extra load margins (horizontal shift) equal to approximately 1/3 of the product of fastener preload and friction efficient, and this fraction increases slightly as the crack tip move away from the fastener.

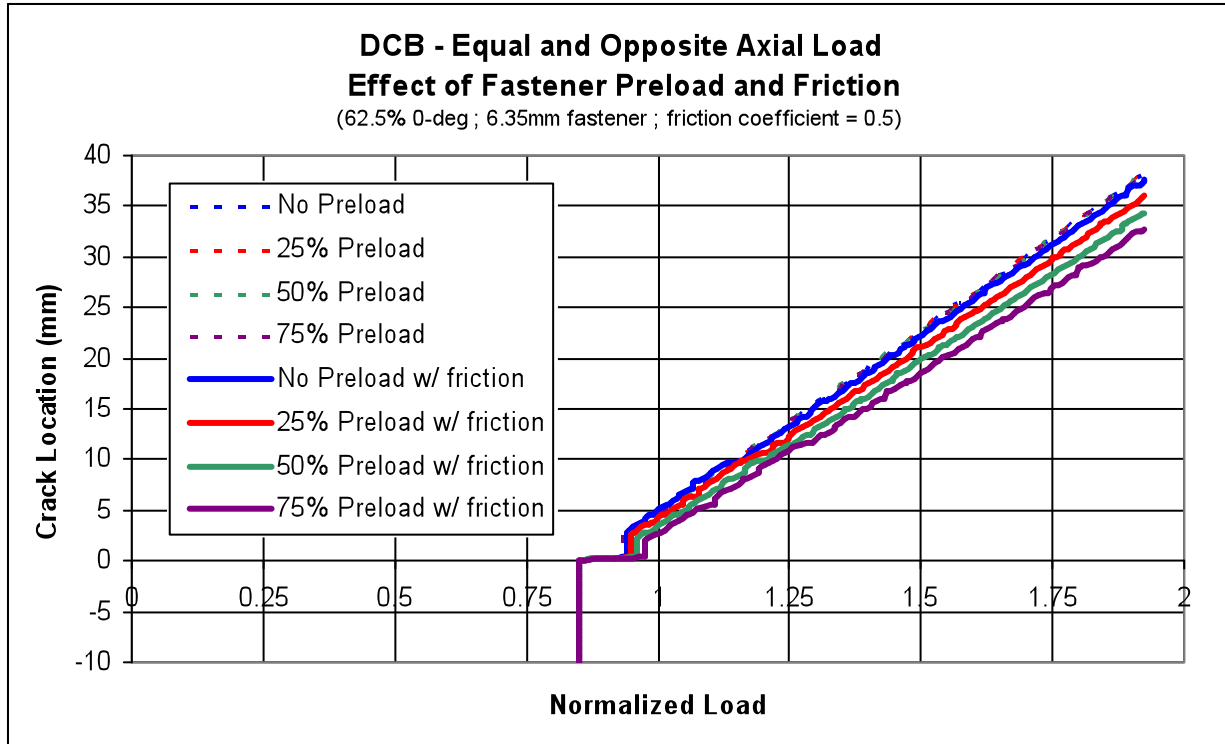


Figure 8. Crack Tip Location vs. Normalized Load – Equal and Opposite Axial Loads

III. Fastener Effectiveness as Disbond Arrest Mechanism – Analytical Modeling

An analytical model for predicting crack propagation behavior of the generalized model shown in Figure 3 is developed using a split-beam model¹⁴ and closed-form mode-decomposed crack tip SERR solution by Wang and Qiao¹¹⁻¹³. The analytical model, shown in Figure 9, consists of two beams, a fastener represented by two springs, and a crack face contact region modeled by an elastic foundation layer. The system equilibrium under arbitrary far-field load is solved using Rayleigh Ritz method (principle of minimum potential energy/PMPE). The force and moment solutions are then used to evaluate the crack tip SERR components to determine crack propagation behavior.

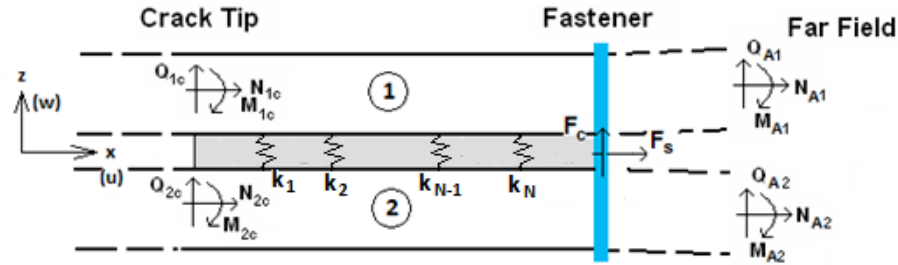


Figure 9. Analytical Model of Split Beam with Fastener ¹⁴

A. Analytical Model

Both axial and bending beam deformations need to be considered, the contact of the cracked faces must be resolved. As the crack propagates, the size of the cracked faces changes, which requires update of the split-beam model. First-order shear deformable beam formulation is used for the two beams to enhance accuracy for short crack lengths. The method for solving equilibrium of the system is a fully analytical approach using principle of minimum potential energy (PMPE) and classical axial stress analysis. Because both axial and bending deformations are considered in this model, there are two options of coupling: linear coupling of axial load with bending stiffness and non-linear coupling of axial and bending deformations. Due to the complexity of analysis of the non-linear coupling, only linear coupling of axial load with bending stiffness is presently considered. The PMPE part of the solution considers beam bending, beam contact, transverse fastener loads, and bending/axial-load coupling. The axial stress analysis part of the solution considers axial deformations and axial fastener loads.

The Rayleigh-Ritz method (PMPE) requires that the displacement functions (w_1 and w_2) be chosen such that the total potential energy (Π) of the system is a minimum, as

well as satisfying the system's boundary conditions. In order to arrive at the correct solution of the system, Equation (3) must be satisfied.

$$\delta\Pi = 0; \text{ where } \Pi = U_T + U_{EL} - W_T \quad (3)$$

The total strain energy, U_T , is the sum of the bending energy, shear energy, strain energy, and bending/axial-load coupling energy, and transverse spring energy. The elastic layer energy, U_{EL} , is the total energy of the springs that model the elastic layer. The total work potential energy, W_T , is the sum of the work potential of the applied transverse loads and applied moments.

The elastic layer is required to prevent penetration of the beams under particular loadings. If the contact of the beams is not resolved then the force and moment solutions will not be valid. The elastic layer is divided into N sections where each section is separated by a spring that has a very large stiffness ($\sim 10^{13}$ N/m) when subjected to compression, and has zero stiffness when subjected to tension; this prevents penetration and allows separation of the beams. The fastener is modeled as two separate springs that act at the beam ends and provide axial and transverse stiffness, respectively. The formulation of the elastic layer energy is shown in Equation (4).

$$U_{EL} = \sum_{n=1}^N \frac{1}{2} k_n (w_2 - w_1)^2 \Big|_{L\left(\frac{n}{N}\right)} \quad (4)$$

The displacement functions for the PMPE of each beam are chosen such that the geometric boundary conditions of the beams are met. The shape functions for the beams, w_1 and w_2 , are shown in Equations (5) and (6), respectively. The limits to the

indices, I and J, are chosen to achieve the desired level of accuracy of the solutions.

The unknowns in the functions are the α_i and β_j terms.

$$w_1 = \sum_{i=1}^I \alpha_i x^{m+1}; \quad i = 1, 2, 3 \dots I \quad (5)$$

$$w_2 = \sum_{j=1}^J \beta_j x^{n+1}; \quad j = 1, 2, 3 \dots J \quad (6)$$

The solutions to w_1 and w_2 are arrived at by simultaneously solving Equations (7) and (8) for the unknown α_i and β_j terms.

$$\frac{\partial \Pi}{\partial \alpha_i} = 0; \quad i = 1, 2, 3 \dots I \quad (7)$$

$$\frac{\partial \Pi}{\partial \beta_j} = 0; \quad j = 1, 2, 3 \dots J \quad (8)$$

Contact is resolved by an iteration scheme that updates the elastic layer spring constants, k_n , based on whether a spring is in tension or compression. If the n^{th} spring is in tension, then $k_n=0$ N/mm for the next loop. If the n^{th} spring is in compression, then $k_n= \sim 10^{10}$ N/mm. The fastener spring constant is determined by material and geometric properties of the fastener when in tension, and is very large ($\sim 10^{10}$ N/mm) when in compression. The iteration continues until the system has converged to the proper displacement. Once the system has converged, then the elastic layer spring forces and transverse fastener/spring force can be determined. The force and moment solutions that act at the crack tip are solved by equilibrium of forces acting on each beam.

For the axial solution, the beams are treated as linear-elastic bars that are attached at the ends by a spring (fastener) that acts in the axial direction only. When the beams are subjected to axial loads the relative displacement of the ends of the beams will

causes a spring force that acts to return the beams ends to their original positions. The stiffness of the fastener in the axial direction is determined by the fastener flexibility approach by Huth⁵ Equilibrium of the beams is arrived at by a closed form solution that solves for the axial spring force due to the relative displacement of the beams ends. From equilibrium the transverse forces that act at the crack tip can be determined.

Once the converged global solution has been obtained, the forces and moments in the beams, fasteners and contact surfaces can be determined. Then, the forces and moments at the crack tip are determined using equilibrium equations. The mode-decomposed crack tip SERR solution¹¹⁻¹³ can then be obtained using the crack tip forces and moments, and crack propagation behavior can be analyzed. As the crack propagates, the length of the model changes, which require an iterative scheme to analyze the crack tip SERR for each crack propagation increment.

The model analyzed is similar to the one shown in Figure 3 described above. Only the 62.5% 0-deg lay-up is used; various fastener diameters were compared. The properties of the fasteners are summarized in Table 4 below. The critical fracture SERR's are $G_{IC} = 0.2627$ N/mm and $G_{IIC} = 1.226$ N/mm. The two load cases considered are 1) equal and opposite transverse shear applied at 63.5mm from the fastener, and 2) equal an opposite axial loads. These load cases are chosen because they will yield pure G_I and G_{II} SERR's at the crack tip respectively (i.e. Mode I and Mode II load cases). For more direct comparison, linear FEA were performed.

Two additional failure modes are considered to better simulate a realistic design environment. Fastener yielding in tension and shear are considered, with failure loads given in Table 4; laminate surface strain failure is considered. A surface strain failure at

5000 μ -strain is assumed, corresponding to a laminate failure load of $Q = 261.5\text{N}$ for load case 1), and $N = 34.7\text{kN}$ for load case 2). Note that in load case 1), since the loads are applied at a distance from the fastener, the loads at the fastener location would be a combination of transverse shear and moment. All loads will be normalized with respect to the laminate surface strain failure loads. The objective of a proper design is such that all other failure modes, such as excessive crack propagation and fastener yield, must occur after the laminate surface strain failure. This applies to other failure modes not considered here, such as fastener pull-through, bearing failure, etc.

Table 4 – Summary of Fastener Properties

Diameter (mm)	k_I (N/mm)	Tensile Yield Load (kN)	k_{II} (N/mm)	Shear Yield Load (kN)
12.7	2.364×10^6	131.0	60.4×10^3	65.5
6.35	591.0×10^3	32.8	38.1×10^3	16.4
3.175	147.8×10^3	8.29	24.0×10^3	4.15
1.5875	36.9×10^3	2.05	15.1×10^3	1.03

B. Results and Discussion – Analytical Model

The results of the analytical model and linear FEA are shown in Figure 10 and 11 below. Crack lengths are plotted against normalized load. Crack lengths are measured from the load application end of the beam to the crack tip; the fastener is located at 63.5mm, thus the arrest mechanism goes into effect when crack length becomes greater than 63.5mm. The loads are normalized against the laminate surface strain

failure load for the respective load case; at normalized load equals to one, the surface strain of the laminates reaches 5000 μ -strain. A vertical line in these plots implies unstable crack propagation. A horizontal line implies no crack propagation. A line with positive slope implies stable crack propagation.

Figure 10 shows the crack propagation behaviors for load case 1) with equal and opposite transverse shear loads, $Q_2 = -Q_1$. When there is no fastener, only a load 0.5 times the laminate failure load would cause catastrophic unstable crack propagation, as indicated by the vertical line. With the presence of a fastener, the load required for crack propagation increases asymptotically for very small crack increments. This is indicative of an extremely well arrested crack, for all fastener diameters considered, from 1.5875mm to 6.35mm. The crack propagation beyond the fastener measures on the order of the fastener size, which is insignificant from a structure point of view. Both FEA and analytical method predicts similar crack growth behaviors. Although the FEA and analytical predictions do not seem to agree with each other perfectly, the actual differences in terms of crack length are very small. The analytical results show a higher degree of sensitivity to the diameter of the fastener than that of the FEA results. For fastener diameter of 1.5875mm, both FEA and the analytical method predict that the fastener will fail in tensile yield at a load of approximately 1.1. The tensile yield predictions for $d = 3.175$ mm do not agree very well with each other.

Figure 11 shows the crack propagation behaviors for load case 2) with equal and opposite axial loads, $N_2 = -N_1$. When there is no fastener, a load of 0.86 times the laminate failure load would cause unstable crack propagation, as indicated by the vertical line. The presence of the fastener induces stable crack growth in the structure

as predicted by both FEA and analytical method, with the stability proportional the diameter of the fastener. The crack arrest effectiveness of the fastener is weaker in this load case, as indicated by higher sloped curves. The crack propagation is on the order of 10mm pass the fastener, which is small on a structure level. The analytical method systematically predicts higher arrest effectiveness (lower slope lines) than the FEA. One known explanation is that the analytical model has yet to include the relative sliding of two crack faces due to bending. When a beam is under bending, the top and bottom surfaces slide relative to the neutral axis by an amount proportional to the rotation of the beam and its thickness. In the FE model, the fastener acts on the displacement between the bottom surface of the upper beam and the upper surface of the bottom beam. However, in the analytical model, such displacement is not modeled because the beams are represented only by their neutral axis. The exclusion of this relative sliding exaggerates the effectiveness of the fastener; modifying the model to include this effect is expected to bring the analytical model closer to that of the FE model. The shear force in the fastener is tracked to determine if the fastener will fail in shear. However, the shear force developed in the fastener is only a fraction of the shear yield load that this failure mode does not appear in Figure 11.

It should be noted that the steps seen in the FEA results in Figure 11 are unexpected, since they do not correspond to any known physical mechanism or event. It is believed that the steps are numerical artifacts from crack propagation simulations. The spring elements that represent the fastener are attached to individual nodes. Significant fastener forces result in concentrated forces at these nodes, which result in excessive local deformations. Since crack propagation by VCCT is dependent on local

crack tip forces and crack opening displacement, these excessive local deformations will impact the accuracy of VCCT when the crack reaches the vicinity of the fastener. In fact, the zone of excessive deformation can clearly be seen in Figure 10, which measures approximately 2.5mm, or 10 finite element lengths in the FE model. However, away from the zone of excessive deformation, the propagation solution is unaffected.

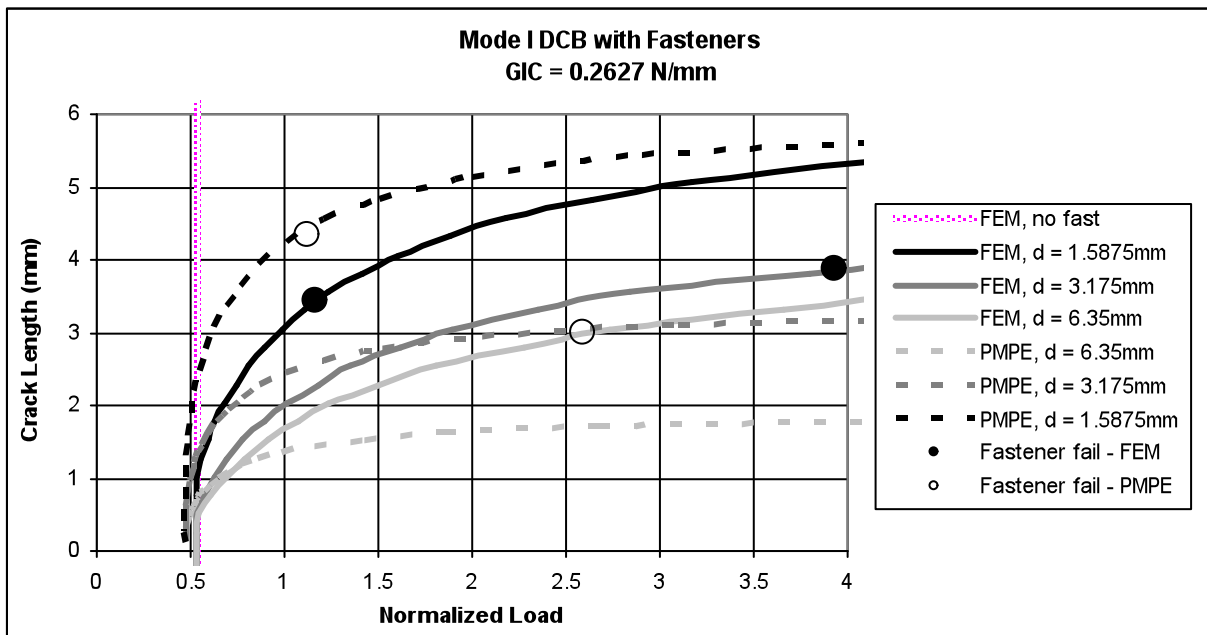


Figure 10. Crack Length vs. Load for Load Case 1 – Equal and Opposite Opening Load

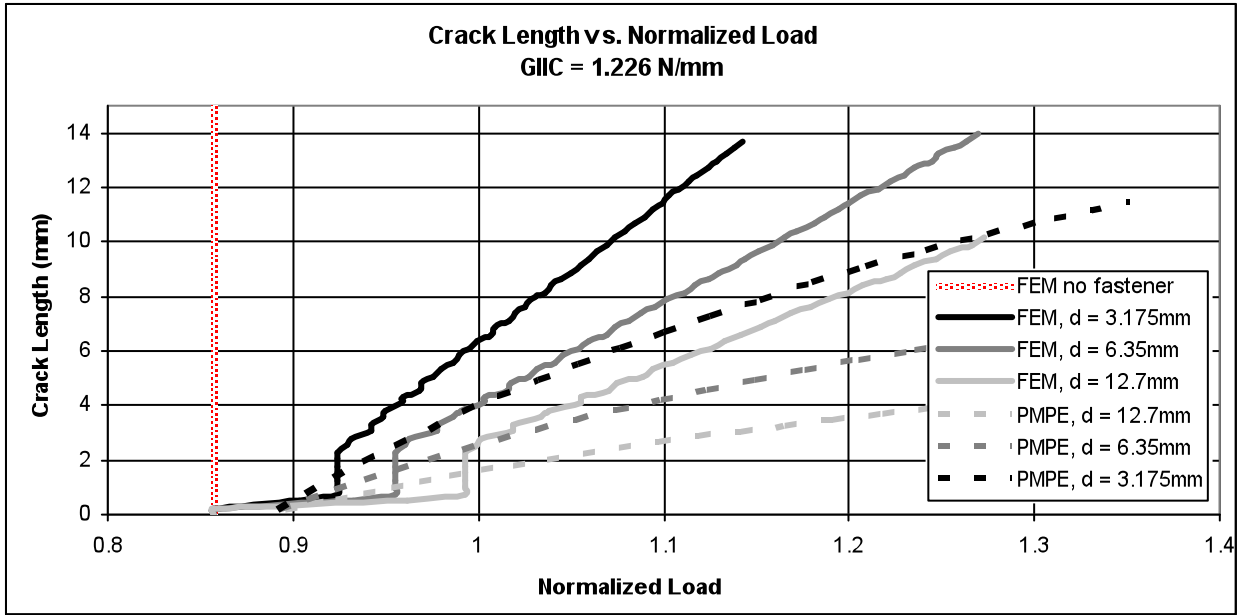


Figure 11. Crack Length vs. Load for Load Case 2 – Equal and Opposite Axial Load

IV. Conclusion

Analysis of effectiveness of fastener as crack arrest feature in composite structure has been demonstrated. In the split-beam FEA model, it is shown that the presence of the fastener is highly effective in arresting the propagation of a crack. The failure load of the arrest mechanism is on average 50% higher than the case where no fastener was present for the pure tension case, and 190% for the pure moment case. It is shown that the fastener effectively eliminates G_I by restricting the opening displacement behind of the crack tip, at the same time forcing the crack to propagate in pure Mode II. The benefit is the highest for load conditions traditionally resulting in the most Mode I SERR component at the crack tip. The load required for crack propagation drastically increases, achieving the desired effect of crack arrestment. In general, the presence of

a fastener-like crack arrest mechanism will turn normally catastrophic unstable crack propagation into a stable one, providing fail-safety to the structure.

An analytical model is developed for the split-beam with fastener configuration, first-order shear deformable beam formulation and mode-decomposed SERR crack tip solution. The solution is obtained using principle of minimum potential energy. The analytical method predicts similar behaviors as the FEA. However, the agreement is limited especially in Mode II case. The omission of interaction between beams with finite thickness is believed to be one of the sources of the error. Modifications to the model shall be made in the future to enhance the accuracy of the predictions. Other failure modes, including laminate surface strain failure and fastener yield, are used to give the problem a more realistic environment and bounds. A proper design of such crack arrest mechanism will take into account all other failure modes such as fastener pull through, bearing failure, etc.

The goal of the current research is to provide designers with a method to analyze the effectiveness of fastener-like crack arrest features. The outcomes of this research will contribute to the design and certification of efficient composite structures. The understanding of crack arrest mechanism may provide an alternative method for repairing damaged structures in operation. A structured approach to solving the problem has been demonstrated. Future work will focus on the development of the analytical method and conducting verification experiments.

Acknowledgments

This work was partially supported by the Federal Aviation Administration Research Grant, Development of Reliability-Based Damage Tolerant Structural Design Methodology. Larry Ilcewicz and Curtis Davies were the FAA grant monitors. The authors wish to thank the FAA Center of Excellence at the University of Washington (AMTAS) for sponsoring the current research project. The Boeing Company also supported the current work. Special thanks are given to Gerald Mabson and Eric Cregger of the Boeing Company for their technical advice and guidance.

References

1. Huang C. and Lin K., "A Method for Reliability Assessment of Aircraft Structures Subject to Accidental Damage," *46th AIAA/ASME/ASCE/AHS/ASC Structures, Structural Dynamics and Materials Conference*, Austin, Texas, Apr. 18-21, 2005.
2. Lin K. and Styuart A., "Probabilistic Approach to Damage Tolerance Design of Aircraft Composite Structures," *AIAA-2006-2156, 47th AIAA/ASME/ASCE/AHS/ASC Structures, Structural Dynamics, and Materials Conference, 14th AIAA/ASME/AHS Adaptive Structures Conference, 7th*, Newport, Rhode Island, May 1-4, 2006.
3. Styuart A. and Lin K. "Maintenance Planning for Aircraft Damage Tolerant Composite Structures Based on Risk Assessment," *AIAA-2007-1979, 48th AIAA/ASME/ASCE/AHS/ASC Structures, Structural Dynamics, and Materials Conference*, Honolulu, Hawaii, Apr. 23-26, 2007.
4. Mabson G. E. and Deobald L. R., "Design Curves for 3D Reinforced Composite Laminated Double Cantilever Beams," *Proc of ASME Int. Mechanical Eng. Congress and Expo.*, 2000. p. 89–99.
5. Huth H., "Influence of Fastener Flexibility on the Prediction of Load Transfer and Fatigue Life for Multiple-Row Joints," *Fatigue in Mechanically Fastened Composite and Metallic Joints, ASTM STP 927, John M. Potter, Ed., American Society for Testing and Materials*, Philadelphia, 1986, pp. 221-250
6. About.com, "Carbon/Graphite Composite Materials," <http://composite.about.com/cs/data//blcarbon.htm> [cited 20th Feb, 2009]

7. Reeder, J., S. Kyongchan, P. B. Chunchu, and D. R.. Ambur, "Postbuckling and Growth of Delaminations in Composite Plates Subjected to Axial Compression" *43rd AIAA/ASME/ASCE/AHS/ASC Structures, Structural Dynamics, and Materials Conference*, Denver, Colorado, vol. 1746, p. 10, 2002.
8. Mabson G., Deobald L. and Dopker B., "Fracture Interface Elements for the Implementation of the Virtual Crack Closure Technique," *AIAA-2007-2376, 48th AIAA/ASME/ASCE/AHS/ASC Structures, Structural Dynamics, and Materials Conference*, Honolulu, Hawaii, Apr. 23-26, 2007.
9. ⁹Freudenthal, A. M., Wang, P.Y., "Ultimate strength analysis of aircraft structures" *Journal of Aircraft*, 1970, 0021-8669 vol.7 no.3 (205-210).
10. Gary P.M., and Riskalla, M.G., "Development of Probabilistic Design Methodology for Composite Structures," *DOT/FAA/AR-95/17*, August 1997.
11. Wang J.L. and Qiao P.H., "On the Energy Release Rate and Mode Mix of Delaminated Shear Deformable Composite Plates," *International Journal of Solids and Structures* 41, 2757-2779, 2004.
12. Qiao P.H. and Wang J.L., "Novel Joint Deformation Models and Their Application to Delamination Fracture Analysis," *Composites Science and Technology* 65, 1826-1839, 2005.
13. Wang J.L. and Qiao P.H., "Fracture Analysis of Shear Deformable Bi-Material Interface," *Journal of Engineering Mechanics*, pp. 306-316, March 2006.
14. Gray P.M., Cheung C.H.E. and Lin K.Y., "Design Tool for Laminated Composite Structures Disbond Arrest Mechanism," *SAMPE 2010 Spring Conference and Exhibition*, Seattle, WA, May 17-20, 2010.